UDK 631.824:537.312.9
Original scientific article/Izvirni znanstveni članek

ISSN 1580-2949
Mater. Tehnol.

EFFECTS OF DIFFERENT LOADING DIRECTIONS ON THE ORGANIZATION AND PROPERTIES OF MAGNESIUM SINGLE CRYSTALS BASED ON MOLECULAR DYNAMICS

ANALIZA VPLIVOV RAZLIČNIH SMERI OBREMENJEVANJA NA ORGANIZACIJO IN LASTNOSTI MAGNEZIJEVIH MONOKRISTALOV S POMOČJO MOLEKULARNE DINAMIKE

Tuo Li, Chuanchuan Ma, Chun Xue, Ri Jin, Yuquan Li, Leifeng Tuo, Hailian Gui, Zhibing Chu*

School of Materials Science and Engineering, Taiyuan University of Science and Technology, Taiyuan 030024, China

Prejem rokopisa – received: 2024-06-08; sprejem za objavo – accepted for publication: 2024-09-30

doi:10.17222/mit.2024.1215

Magnesium and its alloys are widely used as high-quality metal materials in various fields. In this study, the tensile properties of magnesium single crystals under different loading directions were investigated based on the molecular dynamics theory. By analyzing the changes in stress, potential energy, crystal structure, and dislocation lines, the following conclusions can be drawn: There are differences in strain values, dislocation line arrangement laws, and crystal structures of magnesium single crystals when dislocation lines are generated under different loading directions. However, the types of dislocation lines are generally the same, with 1/3 dislocations and dislocations with an unknown structure being dominant. Furthermore, the results indicate that the number of 1/3 dislocations is larger than that of dislocations with an unknown structure. These findings are of great significance for a deeper understanding of the deformation mechanism of magnesium single crystals.

Keywords: molecular dynamics, magnesium single crystal, loading direction, crystal structure, dislocation line density

Magnezij (Mg) in njegove zlitine se široko uporabljajo kot visoko kvalitetni kovinski materiali na različnih področjih. V članku avtorji opisujejo raziskavo nateznih lastnosti Mg mono kristalov pri njihovem obremenjevanju v različnih smereh s pomočjo teorije molekularne dinamike. Na osnovi analize napetostnih sprememb, potencialne energije, kristalne strukture in dislokacijskih linij so prišli do naslednjih ugotovitve: obstajajo različne vrednosti deformacije, zakonov ureditve dislokacijskih linij in kristalnih struktur, ko pride do generiranja dislokacijskih linij zaradi različnih smeri obremenjevanja. Vendar so prevladujoči tipi dislokacijskih linij v splošnem enaki, z 1/3 dislokacijami in dislokacijami neznane strukture. Nadalje rezultati analiz kažejo, da je število dislokacij 1/3 večje kot je število dislokacij z neznano strukturo. Avtorji tudi ugotavljajo, da so njihove ugotovitve zelo pomembne za globje razumevanje deformacijskih mehanizmov Mg mono kristalov.

Ključne besede: molekularna dinamika; mono kristali magnezija; smeri obremenjevanja; kristalna struktura; linijska gostota dislokacij

1 INTRODUCTION

Magnesium and its alloys are widely used as lightweight metallic materials in lightweight structural components in aerospace and other fields. They are considered to be green materials that are resource-efficient and environmentally sustainable.[1–5] Magnesium has advantages such as high specific strength, specific stiffness, and good thermal and electrical conductivity. However, the densely arranged hexagonal crystal (HCP) structure of magnesium single crystals results in high anisotropy of their mechanical properties, which significantly limits the plastic deformation of metals.[6–10] Therefore, it is of great significance to improve the mechanical properties of metals by investigating the changes in the crystal structure of magnesium single crystals during the loading process at a microscopic level.

Selvarajou, Balaji[11] et al. used nanoindentation experiments and crystal plastic finite element (CPFE) simulation to study the orientation-dependent properties of magnesium single crystals under local contact. Monnet Ghiath[12] et al. used molecular dynamics and hydrostatic simulations to investigate the core structure and motion of dislocations in the α-Fe mechanism. Zhang Peng[13] et al. used a molecular dynamics approach to simulate the deformation process of nickel-based single-crystal high-temperature alloys and investigated the effect of the evolution mode of interfacial dislocations and the yield mechanism on the mechanical properties of nickel-based single-crystal high-temperature alloys. V. Kaushik[14] et al. investigated the fracture behavior of magnesium single crystals by experimenting with notched three-point-bending specimens with three crystal orientations. Zhou Nian[15] et al. simulated the nanoindentation of three face-centered cubic (FCC) metals (Al, Cu, and Ni) and two body-centered cubic (BCC) metals (Fe and Ta) using molecular kinetic dynamics and investigated the main types of single-crystal dislocation structures during

*Corresponding author's e-mail:
chuzhibing@tyust.edu.cn (Zhibing Chu)

nanoindentation. Chen Bin[16] et al. used molecular dynamics simulations to investigate the fracture behavior of Ni-based alloys under different impact velocities and the change in the crystal structure. Vasilev Evgenii[17] et al. experimentally investigated the mechanism of the hexagonal close-packed (HCP) to body-centered cubic (BCC) phase transition of magnesium single crystals during plastic deformation. Chao Lou[18] et al. experimentally investigated the local stress induced by the interaction of twinned phases of magnesium single crystals on the microstructural evolution. Mao Lou[19] et al. also experimentally investigated the local stress induced by the interaction of twinned phases of magnesium single crystals on the microstructural evolution.

2 MODEL CONSTRUCTION AND MODELING METHODS

In this paper, the properties of magnesium single crystals under different loading directions are investigated based on molecular dynamics. A magnesium single-crystal model was established using Atomsk software.[20–23] Crystal orientation indices in a densely packed hexagonal structure are expressed in four-axis coordinates, while the model orientation is expressed in three axes, where the *x*, *y*, and *z* coordinates correspond to the [-12-10], [-1010], and [0001] crystal orientations, respectively (as shown in **Figure 1a**. The size of the model created is (12.8 × 22.24 × 20.85) nm, consisting of a total of 256,000 atoms (as shown in **Figure 1b.** Simulations were carried out using the LAMMPS program combined with the tessellated embedded atom method (EAM) potential function. The simulations were conducted under the following conditions: a loading temperature of 300 K, a loading rate of 0.01 s^{-1}, loading directions of *X*, *Y*, and *Z*, and a time step of 0.001 ps until the total strain reached 20 %. By analyzing the stress-strain, potential strain, crystal structure, and dislocation line data from the simulation results, the changes in the performance and deformation mechanisms of single-crystal magnesium under a tensile action in different loading directions were investigated.

3 SIMULATION RESULT ANALYSIS

3.1 Effect of loading direction on the tensile stress-strain relation in magnesium single crystals

Figure 2 shows the stress-strain curves of single-crystal magnesium in tension under different loading directions. From the figure, it can be seen that the stress-strain curves under different loading directions show obvious changes, where the curve changes in the *X* loading direction are obviously different from those in the *Y* and *Z* directions, and the curve movements in the *Y* and *Z* loading directions have the same tendency. The peaks of the curves in the *X*, *Y* and *Z* loading directions increase in turn, and the strain values corresponding to their peaks also increase in turn. The peak point in the *Z* direction is the highest, and can reach 2.18 GPa, corresponding to 10.5 % of the strain, followed by the peak point in the *Y* direction, which is 1.20 GPa, corresponding to 9.2 % of the strain, and the peak point of the stress in the *X* loading direction, which is 0.43 GPa, corresponding to 3.9 % of the strain. It can be seen that the stress and strain values are minimum in the *X* direction and maximum in the *Z* direction. The main reason for this phenomenon is the fact that magnesium single crystals have a dense hexagonal crystal structure.

Under a tensile load, the first change in the slip system is different for different loading directions. The crystal change in the *X* loading direction occurs along the densest row of surfaces in the hexagonal crystal structure, which corresponds to the easiest slip system. Therefore, the required stress in the *X* loading direction is small. The crystal change in the *Y* loading direction occurs along a dense row of surfaces in the hexagonal crystal structure, but it does not correspond to the easiest slip system. Therefore, the required stress in the *Y* loading direction is higher than that in the *X* loading direction. The crystal change in the Z loading direction occurs along the prismatic face of the magnesium single crystal,

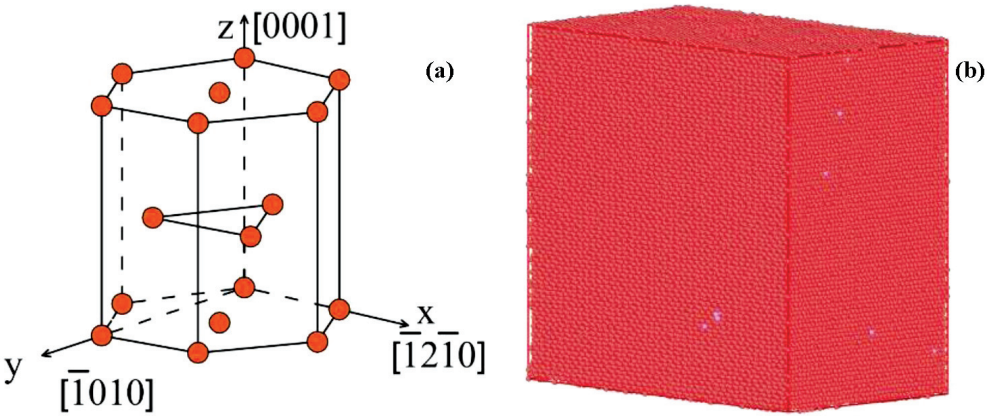

Figure 1: a) Atomic model diagram of magnesium and b)magnesium single-crystal model

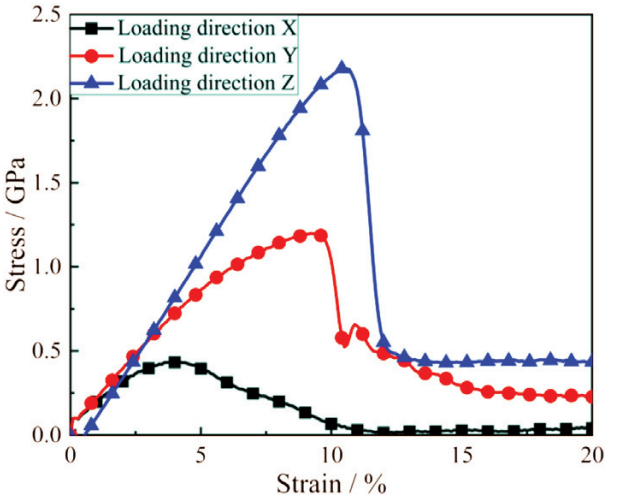

Figure 2: Stress-strain curves under three loading directions

which does not correspond to the densest row of surfaces in the hexagonal crystal structure. Therefore, the required stress in the *Z* loading direction is the highest among the three directions, and the change is the most significant.

3.2 Effect of loading direction on the tensile potential energy-strain relation of magnesium single crystals

Figure 3 shows the corresponding potential energy-strain curves for a single crystal of magnesium stretched under different loading directions. From the figure, it can be seen that after a systematic chirp, the potential energy returns to the same initial value when it is not stretched. When loading along the X direction, the potential energy reaches its maximum value at 9 %, which is –378.21 keV. When loading along the Y direction, the potential energy reaches its maximum value at 9.5 %, which is –371.51 keV. When loading along the Z direction, the potential energy reaches its maximum value at 11 %, which is –365.46 keV. Considering **Figure 2** as well, it can be observed that the corresponding

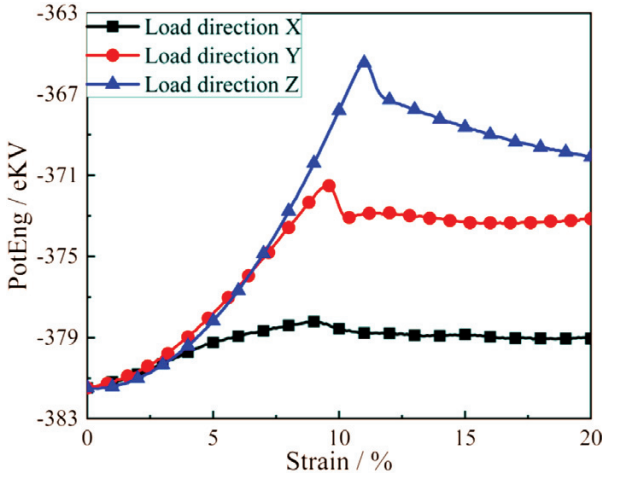

Figure 3: Potential energy strain curves under three loading directions

values of strain and potential energy are lower when loading along the *X* direction. These lower values are mainly achieved because the magnesium single crystal is more prone to change in this direction. The higher absolute values of the strain and potential energy in the *Z* loading direction are due to the fact that the *Z* loading direction is not the most likely crystallographic direction for dense hexagonal rows, and more energy is required to break the metal bonds.

3.3 Effect of loading direction on the change of crystal structure of magnesium single crystals

In the crystal structure, the arrangement of atoms determines various properties of the material, including electronic structure and mechanical properties. In magnesium single crystals, there are strong metallic bonds between the atoms in their crystal structure, giving magnesium single crystals good electrical and thermal conductivity. Additionally, the crystal structure of magnesium single crystals determines their mode of plastic deformation. Due to the uniqueness of their hexagonal closest packing (HCP) structure, magnesium single crystals undergo dislocation slip during plastic deformation. Under ambient conditions, magnesium single crystals adopt a HCP crystal structure; however, as the loading process continues, the HCP structure of magnesium single crystals is transformed into an FCC or BCC structure.[24,25] For this reason, the study of the HCP crystal structure transformation is important to understand the mechanical properties of the material and its deformation behavior under strain loading.[26–31]

Figure 4 shows the number of different crystal structures versus strain at different loading directions. **Figure 4a** represents the *X* loading direction, **Figure 4b** represents the *Y* loading direction, and **Figure 4c** represents the *Z* loading direction. The five values of strain in **Figures 4d** to **4f** correspond to the beginning of strain, the strain corresponding to the yield point, the strain corresponding to the same number of HCP and OTHER structures, the 15-% strain, and the 20-% strain, respectively.

In **Figure 4a**, the HCP structure is first transformed into BCC and OTHER structures. The HCP structure decreases sharply, and the BCC structure increases dramatically at a strain of 3.9 %. The HCP structure has the same number as the BCC structure at 7.2 %, which is the inflection point. The number of BCC structures is larger than the number of HCP structures. At 9.4 %, the HCP structure starts to reappear, the BCC structure starts to decrease, and the FCC structures begin to appear and gradually increase. The OTHER structures exist in a smooth form after their appearance. In **Figure 4b**, the HCP structures are first transformed into OTHER structures, then the BCC structures appear, and finally the FCC structures appear. The OTHER structure becomes obvious at 5.4-% strain and gradually increases. The BCC structure increases significantly at 8.9 % and starts

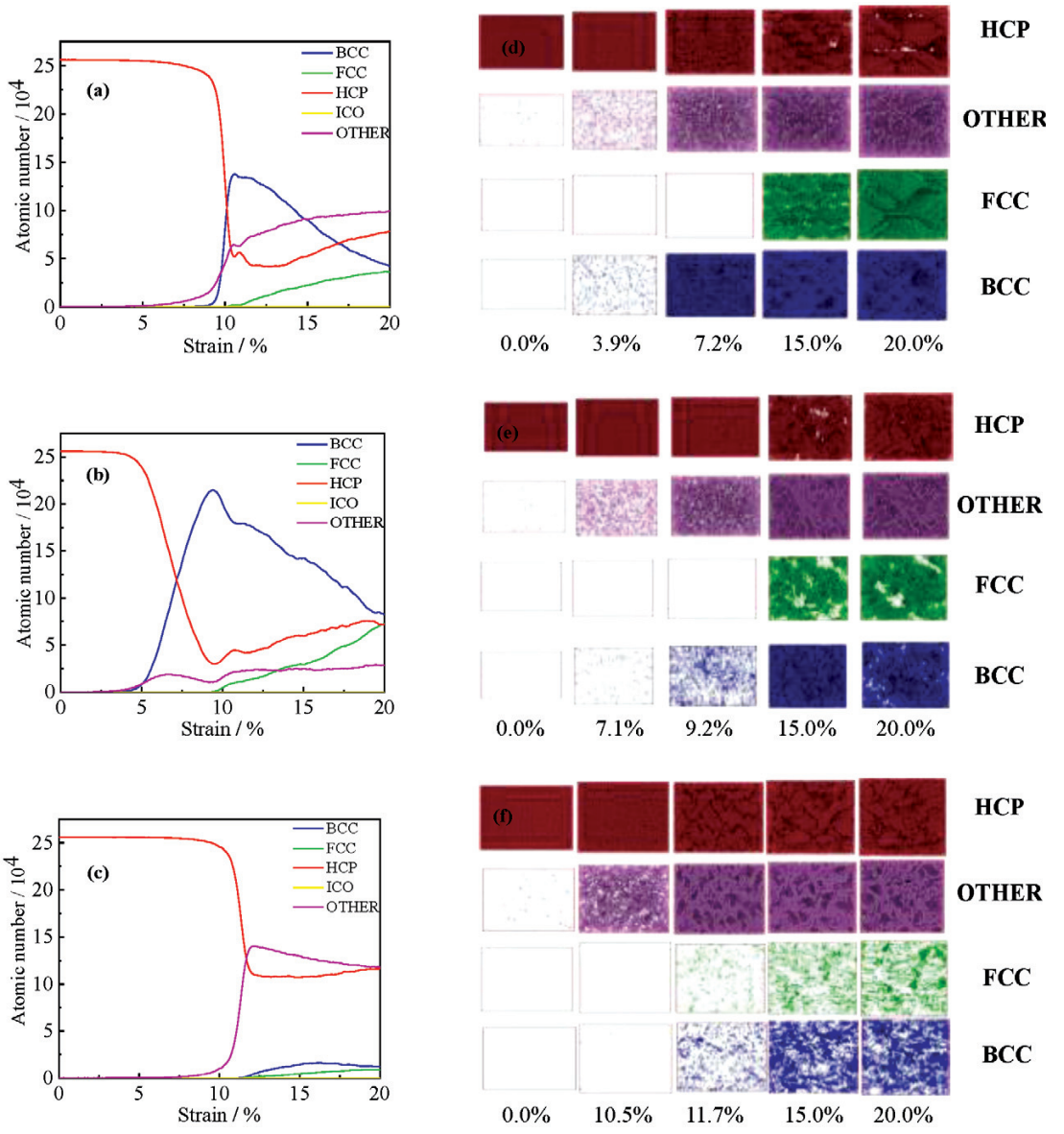

Figure 4: Crystal structure change curves and structure diagrams; a), b), c) show the crystal change curves under different loading directions; d), e), f) show the crystal structures under different strains

to decrease at 10.8 %. At this time, the HCP structure fluctuates slightly, but the overall trend is considered to be decreasing, while the FCC structure arises and increases gradually. At 12.6 %, the HCP structure starts to recover slowly and finally tends to become flat. In **Figure 4c**, before the stress peak, the HCP structure is first transformed into the OTHER structure. After the stress peak, the FCC and BCC structures begin to appear, while the OTHER structure starts to decrease, and then reaches a relative equilibrium state. The HCP structure recovers slightly and then tends to level off. It can be seen that when acting in the X loading direction, it is easier to be converted to the BCC structure to promote motion. When acting in the Z loading direction, it is converted to an unknown structure, which has no obvious effect on the promotion of motion.

Figure 5 shows the corresponding crystal structure changes at different strains in different directions. The first picture corresponds to different loading directions and represents the beginning of the crystal structure changes in that loading direction. The second picture represents the beginning of the crystal structure changes in the next loading direction. The third and fourth pictures represent the crystal structure changes in different loading directions when the corresponding strains are 15 % and 20 %, respectively. The green color represents the FCC structure, the red color represents the HCP structure, the blue color represents the BCC structure, the yellow color represents the ICO structure, and the white color represents the OTHER structure. From the figure, it can be seen that as the strain progresses, the HCP structure is increasingly converted into other crystal

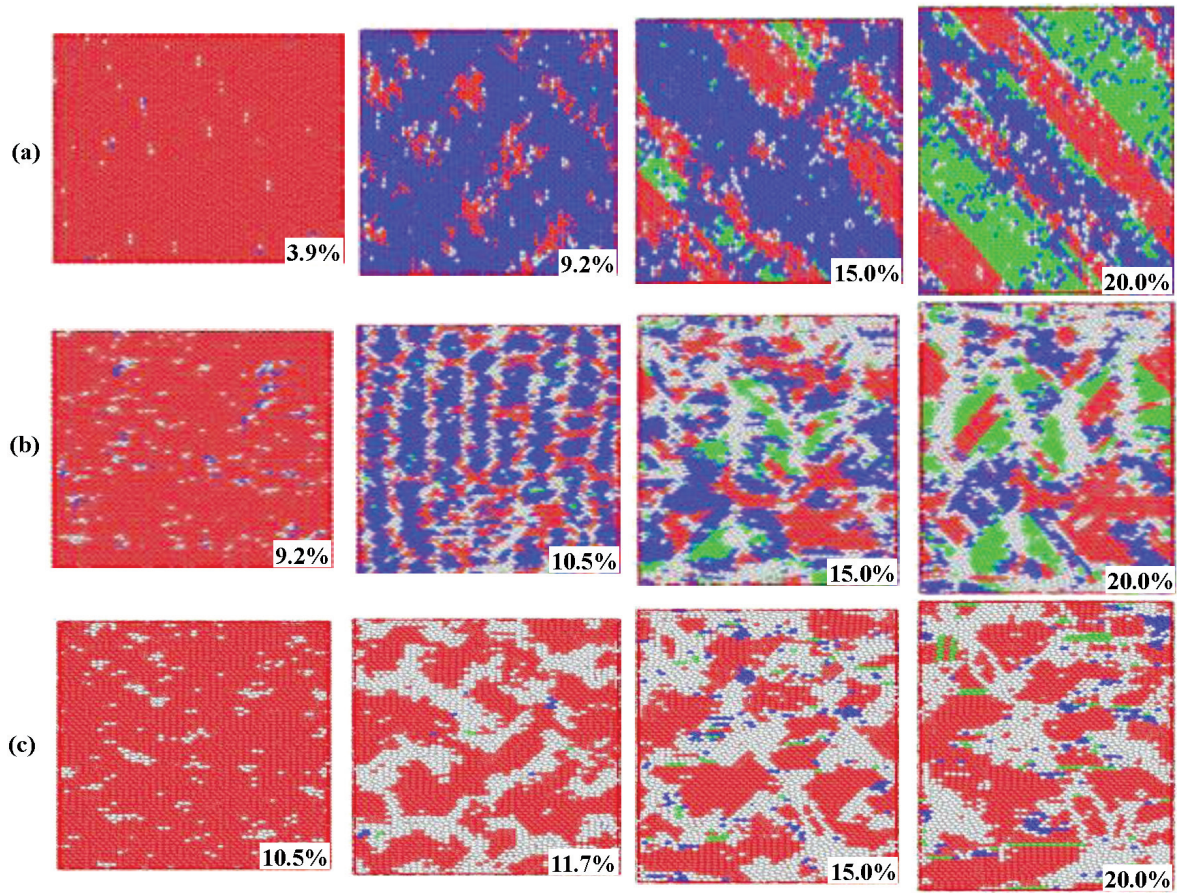

Figure 5: a), b) and c) show the crystal structure changes under different strains in *X*, *Y* and *Z* loading direction, respectively

structures. When loading in the *X* direction, a disordered unknown structure starts to appear and is then converted into a large area of the BCC structure. It gradually transitions into a regular distribution accompanied by the generation of FCC structures. In the *Y* direction, there is initial generation of relatively regular turbulence points. As the strain progresses, the HCP structure is converted into a regular distribution of BCC structure and an irregular distribution of OTHER structure. At higher strains, the number of BCC structures decreases, the number of OTHER structures increases, and FCC structures are generated. The crystal exhibits an overall irregular distribution with local regularity. In the *Z* loading direction, there are irregular disordered points at the beginning. Then, the HCP structures are mainly converted into OTHER structures, and a small number of BCC and FCC structures gradually appear. Finally, the crystal shows an overall irregular distribution with local regularity. It can be seen that in the *X* loading direction, the crystal structure is mainly BCC structure, and it is regular. In the *Y* loading direction, the main structure is BCC, and as the strain progresses, there are more FCC structures and unknown structures, resulting in an overall irregular distribution with local regularity. In the *Z* loading direction, the dominant structure is an unknown structure, and as the strain proceeds, small amounts of BCC and FCC

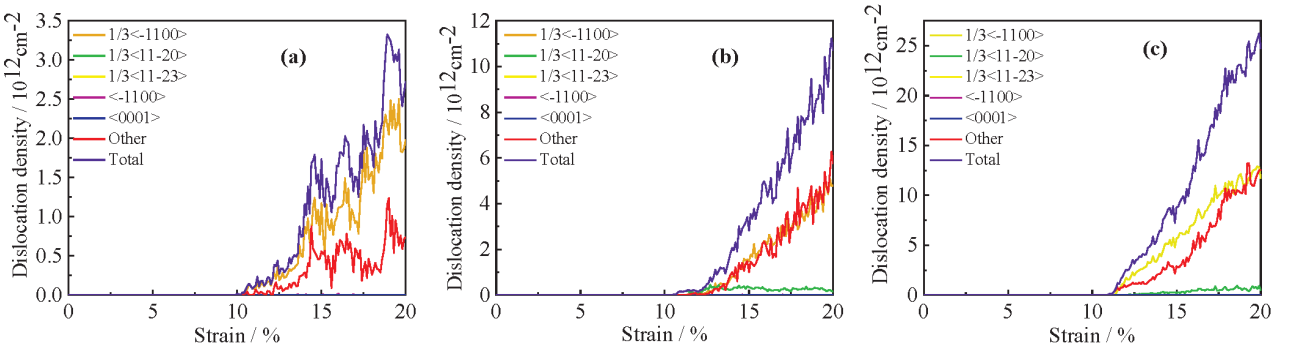

Figure 6: a), b), and c) represent strain-dislocation density curves at *X*, *Y*, and *Z* loading directions, respectively

structures appear, resulting in an overall irregular distribution with local regularity.

3.4 Effect of loading direction on the variation of magnesium single-crystal dislocation curves

The plots of dislocation density versus strain for different loading directions are given in **Figure 6**, where **Figure 6a** shows the X loading direction, **Figure 6b** shows the Y loading direction, and **Figure 6c** shows the Z loading direction. We can see that the types of dislocations appearing under tensile loading in different loading directions are: 1/3, 1/3, 1/3, , and dislocations, and that there are also some unidentifiable dislocations, defined as other dislocations. From the figure we can see that the overall trend of each dislocation is converging with strain, where the density of dislocation lines is the smallest in the X direction and the density of dislocation lines is the largest in the Z direction. In **Figure 6a**, dislocations start to appear at a strain of 10.2 %, with the dominant role played by 1/3 dislocations and other dislocations. The overall trend of these two kinds of dislocations is increasing, but the fluctuation is larger as the strain progresses. The number of 1/3 dislocations is larger than that of other dislocations. In **Figure 6b**, dislocations start to be generated at 10.7 % strain and gradually increase with the strain. The dominant types are 1/3 and other dislocations, with their numbers being basically the same. Additionally, a small number of 1/3 dislocations are generated and their number tends to stabilize during the straining process. In **Figure 6c**, at a strain of 11.3 %, there are dislocations, mainly consisting of 1/3 dislocations and other dislocations. Both types of dislocations are gradually increasing, with the number of 1/3 dislocations always being larger than that of the other dislocations. The 1/3 dislocations are generated at 12.3 %, and their number tends to stabilize as the strain progresses. It can be seen that the 1/3 dislocations and other dislocations play a dominant role in different loading directions with the strain, in which the number of 1/3 dislocations is larger than that of other dislocations, and the 1/3 dislocations play a secondary role, not determining the direction of strain occurrence.

Figure 7 shows variation curves of dislocation density with strain under different loading directions. The first graph represents dislocation line graphs under the corresponding strain when dislocations are generated, while the second graph represents dislocation line graphs corresponding to the strain when dislocations are generated in the next loading direction. The third and fourth graphs correspond to dislocation line graphs under the strains of 15 % and 20 %, respectively. From the graphs, we can observe that the dislocation line density increases to varying degrees as the strain progresses under different loading directions. In the *X* loading direction, the dislocation lines start to be generated at 10.2 % strain, and their distribution is disordered. As the strain progresses, dislocation lines grow and their number gradually in-

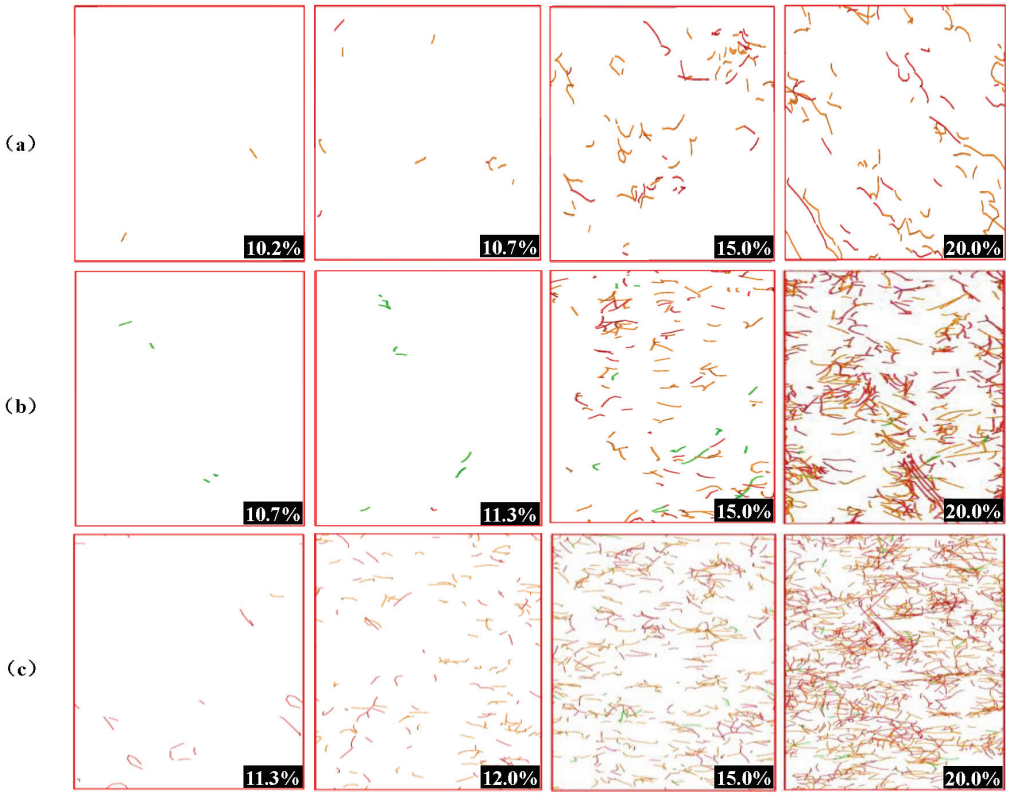

Figure 7: a), b), and c) represent the change in the dislocation line under the *X*, *Y* and *Z* loading direction, respectively

creases, eventually showing a regular distribution. This is mainly because in the *X* loading direction, dislocations are generated along the direction where the crystal is prone to change, requiring less energy and producing less stress. This results in fewer atomic structure disruptions and corresponds to a lower number of dislocations. In the *Y* loading direction, dislocation lines start to be generated at 10.7 % strain, and their distribution is disordered. As the strain increases, the dislocation lines grow, merge, and split, eventually exhibiting an overall irregular and locally regular distribution at larger strains. In the *Z* loading direction, dislocation lines start to be generated at 11.3 % strain, and they have a longer length. Initially, the dislocation lines have a more orderly distribution with increasing strain. However, as the dislocations continue to occur, the dislocation lines grow, intertwine, and eventually show an overall irregular and locally more regular distribution.

It can be observed that in the *X* loading direction, there are fewer dislocation lines, but their distribution is regular. In the *Y* loading direction, there are more dislocation lines compared to the *X* loading direction, and they have longer lengths. However, the distribution of these dislocation lines is overall disordered with some local order. In the *Z* loading direction, there are more dislocation lines than in both the *X* and *Y* loading directions. These lines are long and interwoven, resulting in an overall disorder with a relatively more orderly local order.

4 CONCLUSIONS

In this paper, the changes in the properties of magnesium single crystals under different loadings at 300 K are investigated using molecular dynamics. The following results are obtained by discussing the stress strain, potential energy strain, dislocation line changes and crystal structure changes:

1) The strain values corresponding to the generation of dislocation lines in magnesium single crystals under different loading directions are different, with the smallest strain value corresponding to the *X* direction, followed by the *Y* direction, and *Z* direction with the largest strain value.

2) Under different loading directions, the arrangement of dislocation lines and the conversion and distribution of the crystal structure vary. When loaded in the *X* direction, dislocation lines are regularly distributed, and most of the HCP structure converts into the BCC structure. When loaded in the *Y* direction, the overall distribution of dislocation lines is irregular with some local regularity, and the crystal structure undergoes conversion primarily into the BCC structure, along with some OTHER structure. When loaded in the *Z* direction, the overall distribution of dislocation lines is irregular with some local regularity, and the HCP structure mainly converts into an unknown structure.

3) Under different loading directions, the number and length of dislocation lines are different. In the *X* direction, the number of dislocation lines is small and the lines are short. In the *Y* direction, there are more and longer dislocation lines accompanied by a small amount of interweaving. In the *Z* direction, the number of dislocation lines is large, the lines become longer and there is a lot of interweaving. The types of dislocation lines are basically the same; 1/3 dislocation and unknown structure dislocation play a dominant role, and the 1/3 dislocation number is greater than that of the unknown structure dislocation.

Acknowledgement

This work was supported by the National Natural Science Foundation of China (52175353), and the Shanxi Province Key Research and Development Programme Project (202102150401002).

5 REFERENCES

[1] J. F. Song, J. She, D. L. Chen, Latest research advances on magnesium and magnesium alloys worldwide, Journal of Magnesium and Alloys, 8 (**2020**) 1, 1–41, doi:10.1016/j.jma.2020.02.003

[2] Y. Yang, X. M. Xiong, J. Chen, Research advances in magnesium and magnesium alloys worldwide in 2020, Journal of Magnesium and Alloys, 9 (**2021**) 3,705–747, doi:10.1016/j.jma.2021.04.001

[3] Y. Ali, D. Qiu, B. Jiang, Current research progress in grain refinement of cast magnesium alloys: A review article, Journal of Alloys and Compounds, 619 (**2015**), 639–651, doi:10.1016/j.jallcom.2014.09.061

[4] K. Luo, L. Zhang, G. H. Wu, Effect of Y and Gd content on the microstructure and mechanical properties of Mg–Y–RE alloys, Journal of Magnesium and Alloys, 7 (**2019**) 2, 345–354, doi:10.1016/j.jma.2019.03.002

[5] M. Yeganeh, N. Mohammadi, Superhydrophobic surface of Mg alloys: A review, Journal of Magnesium and Alloys, 6 (**2018**) 1, 59–70, doi:10.1016/j.jma.2018.02.001

[6] J. F. Deng, J. Tian, Y. Y. Chang, The role of š10–12ć tensile twinning in plastic deformation and fracture prevention of magnesium alloys, Materials Science & Engineering A, 853 (**2022**), doi:10.1016/j.msea.2022.143678

[7] A. Rezaei, R. Mahmudi, C. Cayron, Simple shear extrusion versus equal channel angular pressing: A comparative study on the microstructure and mechanical properties of an Mg alloy, Journal of Magnesium and Alloys, 11 (**2023**) 5, doi:10.1016/j.jma.2023.05.006

[8] J. K. Feng, D. F. Zhang, H. J. Hu, Improved microstructures of AZ31 magnesium alloy by semi-solid extrusion, Materials Science & Engineering A, 800 (**2021**), doi:10.1016/j.msea.2020.140204

[9] K. Raineesh, P, Prasad, K Eswar, Indentation size effect in magnesium single crystals of different crystallographic orientations, Journal of Materials Research, 37 (**2022**) 3, doi:10.1557/s43578-021-00480-3

[10] Z. Liu, E. Simonetto, A. Ghiotti, Mechanical Behaviour of Magnesium Alloy Based - Fiber Metal Laminates after Fabrication Using Different Metal Surface Treatments, Key Engineering Materials, 926 (**2022**), 1327–1335. doi:10.4028/p-5me991

[11] B. Selvarajou, J. H. Shin, T. K. Ha, Orientation-dependent indentation response of magnesium single crystals: Modeling and experiments, Acta Materialia, (**2014**) 81, 358–376, doi:10.1016/j.actamat.2014.08.042

[12] G. Monnet, D. Terentyev, Structure and mobility of the 1/2 < 111 > {112} edge dislocation in BCC iron studied by molecular dynamics, Acta Materialia, 57 (**2009**) 5, 1416–1426, doi:10.1016/j.actamat.2008.11.030

[13] P. Zhang, L. F. Zhang, Q. Zhu, Interfacial dislocation evolution and yield mechanism of nickel-based single crystal superalloy: A molecular dynamics research, Materials Today Communications, 32 (**2022**), doi:10.1016/j.mtcomm.2022.104006

[14] V. Kaushik, R. Narasimhan, R. K. Mishra, Experimental study of fracture behavior of magnesium single crystals, Materials Science & Engineering A, (**2014**) 590, 174–185, doi:10.1016/j.msea.2013.10.018

[15] N. Zhou, K. I. Elkhodary, X. X. Huang, Dislocation structure and dynamics govern pop-in modes of nanoindentation on single-crystal metals, Philosophical Magazine, 100 (**2020**) 12, 1585–1606, doi:10.1080/14786435.2020.1739348

[16] B. Chen, W. P. Wu, Molecular dynamics simulations of dynamics mechanical behavior and interfacial microstructure evolution of Ni-based single crystal superalloys under shock loading, Journal of Materials Research and Technology, 15 (**2021**), 6786–6796, doi:10.1016/j.jmrt.2021.11.116

[17] E. Vasilev, D. Popov, M. Somayazulu, White Laue and powder diffraction studies to reveal mechanisms of HCP-to-BCC phase transformation in single crystals of Mg under high pressure, Scientific Reports, 13 (**2023**) 1, doi:10.1038/s41598-023-29424-z

[18] C. Lou, J. P. Yu, L. Liu, {10-12} twin nucleation induced by FIB micro-stress in magnesium single crystal, Materials Letters, 210 (**2018**), doi:10.1016/j.matlet.2017.09.031

[19] P. Hirel, Atomsk: A tool for manipulating and converting atomic data files, Computer Physics Communications, 197 (**2015**), 212–219, doi:10.1016/j.cpc.2015.07.012

[20] C. Mieszczynski, P. Jozwik, K. Skrobas, Combining MD-LAMMPS and MC-McChasy2 codes for dislocation simulations of Ni single crystal structure, Nuclear Instruments and Methods in Physics Research Section B: Beam Interactions with Materials and Atoms, 540 (**2023**), 38–44, doi:10.1016/j.nimb.2023.04.01

[21] H. S. Jang, D. Seol, B. J. Lee, Modified embedded-atom method interatomic potentials for Mg–Al–Ca and Mg–Al–Zn ternary systems, Journal of Magnesium and Alloys, 9 (**2021**) 1, 317–335, doi:10.1016/j.jma.2020.09.006

[22] W. Huang, K. L. Pan, J. Zhang, Strain Rate and Temperature Effects on Tensile Properties of Polycrystalline Cu6Sn5 by Molecular Dynamic Simulation, Crystals, 11 (**2021**) 11, 15, doi:10.3390/cryst11111415

[23] H. S. Jang, K. M. Kim, B. J. Lee, Modified embedded-atom method interatomic potentials for pure Zn and Mg-Zn binary system, Calphad, 60 (**2018**), 200–207, doi:10.1016/j.calphad.2018.01.003

[24] Q. Zhang, Selective control of fcc and hcp crystal structures in Au-Ru solid-solution alloy nanoparticles, Nature Communications, 9 (**2018**) 1, doi:10.1038/s41467-018-02933-6

[25] G. Kaptay, On the Order-Disorder Surface Phase Transition and Critical Temperature of Pure Metals Originating from BCC, FCC, and HCP Crystal Structures, International Journal of Thermophysics, 33 (**2012**) 7, 1170–1190, doi:10.1007/s10765-012-1270-5

[26] X. J. Li, Y. Qin, J. Fu, A Gupta potential for magnesium in hcp phase, Computational Materials Science, 98 (**2015**), 328–332, doi:10.1016/j.commatsci.2014.11.023

[27] R. Becker, J. T. Lloyd, A reduced-order crystal model for HCP metals: Application to Mg, Mechanics of Materials, 98 (**2016**), 98–110, doi:10.1016/j.mechmat.2016.04.009

[28] B. M. Morrow, E. K. Cerreta, R. J. McCabe, Toward understanding twin-twin interactions in hcp metals: Utilizing multiscale techniques to characterize deformation mechanisms in magnesium, Materials Science and Engineering A, 613 (**2014**), 365–371, doi:10.1016/j.msea.2014.06.062

[29] S. Rawat, N. Mitra, Twinning, phase transformation and dislocation evolution in single crystal titanium under uniaxial strain conditions: A molecular dynamics study, Computational Materials Science, 172 (**2020**), doi:10.1016/j.commatsci.2019.109325

[30] R. Thevamaran, C. Griesbach, S. Yazdi, Dynamic martensitic phase transformation in single-crystal silver microcubes, Acta Materialia, 182 (**2020**), 131–143, doi:10.1016/j.actamat.2019.10.006

[31] Q. Zu, Y. F. Guo, X. Yao, Surface and orientation effects on stress-induced hcp-fcc phase transformation in Ti nanopillars, Applied Surface Science, 509 (**2020**), doi:10.1016/j.apsusc.2019.145234